ISTANBUL TECHNICAL UNIVERSITY ★ INSTITUTE OF SCIENCE AND TECHNOLOGY

ELECTROMAGNETIC IMAGING OF DIELECTRIC ROUGH INTERFACES

M.Sc. Thesis by
Çağla TAŞDEMİR, B.Sc.

Department : Electronics and Communication Engineering

Programme : Telecommunication Engineering

JUNE 2008

ISTANBUL TECHNICAL UNIVERSITY ★ INSTITUTE OF SCIENCE AND TECHNOLOGY

ELECTROMAGNETIC IMAGING OF DIELECTRIC ROUGH INTERFACES

M.Sc. Thesis by
Çağla TAŞDEMİR, B.Sc.
(504061313)

Date of submission : 05 May 2008
Date of defence examination: 11 June 2008

Supervisor (Chairman) : Prof. Dr. İbrahim AKDUMAN (ITU)
Members of the Examining Committee : Assoc. Prof. Dr. Ali YAPAR (ITU)
Assis. Prof. Dr. Lale Tükenmez ERGENE (ITU)

JUNE 2008

İSTANBUL TEKNİK ÜNİVERSİTESİ ★ FEN BİLİMLERİ ENSTİTÜSÜ

DİELEKTRİK ARAYÜZEYLERİN ELEKTROMANYETİK GÖRÜNTÜLENMESİ

YÜKSEK LİSANS TEZİ
Müh. Çağla TAŞDEMİR
(504061313)

Tezin Enstitüye Verildiği Tarih : 05 Mayıs 2008
Tezin Savunulduğu Tarih : 11 Haziran 2008

Tez Danışmanı : Prof. Dr. İbrahim AKDUMAN (İTÜ)
Diğer Jüri Üyeleri : Doç. Dr. Ali YAPAR (İTÜ)
Yrd. Doç. Dr. Lale Tükenmez ERGENE (İTÜ)

HAZİRAN 2008

ACKNOWLEDGEMENT

I would like to express my immense gratitude to Prof. Dr. İbrahim AKDUMAN, who gave me the opportunity to do research under his supervision and I would also like to thank to Assoc. Prof. Ali YAPAR, not only guided me on this thesis, but also helped me improve my perspective.

I owe my thanks to TÜBİTAK for their support in during my master education and also I would like to thank to my parents and my sister for supporting and encouraging me throughout my life.

June, 2008 **Çağla TAŞDEMİR**

TABLE OF CONTENTS

ABBREVIATIONS

NDT **:** Non-Destructive Testing
PEC **:** Perfect Electric Conductor

LIST OF FIGURES

Page Number

LIST OF SYMBOLS

ω	: Angular frequency
Γ_d	: Destructed surface
ε_0	: Dielectric permittivity of the free space
μ_0	: Magnetic permeability of the free space
$\varepsilon_1, \varepsilon_2$	: Relative dielectric permittivities of the first and second media respectively
σ_1, σ_2	: Conductivities of first and second media respectively
k_1, k_2	: Wavenumber of the first and second media respectively.
Φ_0	: Incident angle
u^i	: Incident field
u^s	: Scattered field
M, N	: Truncation numbers in Taylor expansions
K^*	: L^2 adjoint of the operator K
α	: Regularization parameter
f	: Surface variation
F_M'	: Frechet derivative of operator F
Δf	: Change in surface variation

ELECTROMAGNETIC IMAGING OF DIELECTRIC ROUGH INTERFACES

SUMMARY

In this thesis, electromagnetic imaging of dielectric rough interfaces is presented with simulation results. The subject is presented in two cases: First, dielectric rough surface located over a perfectly conducting plane is reconstructed and second, dielectric surface beyond a layered media is reconstructed using the same method. Considering surfaces having variation only in one space dimension, plane electromagnetic wave with a fixed frequency is used for excitation. Scattered field measurements on a paralel line above the surface to be reconstructed are used and a special representation of the scattered field in terms of Fourier Transform and Taylor expansion is used in boundary conditions which leads to the solution of a system of nonlinear equations where Newton Method is applied iteratively with some kind of regularization. In this study, Tikhonov regularization is applied. In addition, in some cases, least square regularization is applied in order to get more accurate results. The simulation results are discussed with the effects of parameters used in the problems. These parameters are iteration number, truncation parameter used in Taylor expansion, regularization parameter, incident angle of the plane elecromagnetic wave and noise level. Finally it can be shown that, satisfactory results are obtained in reconstructing the defects on the surfaces with the amplitude of $\lambda/200$ in both problems and the method can be effectively used in non-destructive testing of materials which is an important subject in the inverse scattering theory with its wide range of practical applications.

DİELEKTRİK ARAYÜZEYLERİN ELEKTROMANYETİK GÖRÜNTÜLENMESİ

ÖZET

Bu tezde, engebeli dielektrik arayüzlerin elektromanyetik görüntülenmesi üzerinde çalışılmıştır. Konu iki bölümde ele alınmıştır: İlk olarak mükemmel iletken düzlem üzerindeki dielektrik yüzeyin elde edilmesi problemi incelenmiştir, ikinci olarak ise üzerinde dielektrik katmanlar bulunan dielektrik yüzeyin elde edilmesi problemi aynı metot ile incelenmiştir. Tek boyutta değişimlerin olduğu yüzeylerin sabit frekanslı düzlemsel dalgalar tarafından aydınlatıldığı durum göz önüne alınmıştır. Hesaplanacak yüzeyin üzerinde kalan bölgede ve yüzeye paralel bir çizgi üzerindeki saçılan alan ölçümleri problemin çözümünde kullanılacaktır. Saçılan alan Fourier Dönüşümü ve Taylor Açılımı ile ifade edilir; problemin çözümü sınır koşulları kullanılarak elde edilen lineer olmayan denklem sisteminin çözümüne indirgenir. Denklem sisteminin çözümünde ise Newton Metodu yinelemeli bir şekilde uygulanırken regularizasyon uygulanmasını gerektirir. Bu çalışmada Tikhonov Regularizasyonu uygulanmıştır. Ayrıca, daha doğru sonuçlar elde edilmesi için kimi durumlarda En Küçük Kareler Yöntemi kullanılmıştır. Benzetim sonuçları, problemde kullanılan parametrelerin etkisine bağlı olarak incelenmiştir. Bu parametreler iterasyon sayısı, Taylor Açılımında kullanılan terim sayısı, regularizasyon parametresi, düzlemsel dalganın geliş açısı ve gürültü seviyesidir. Sonuç olarak iki problem için de $\lambda/200$ genlikli hasarların bile tespit edilebildiği gösterilmiştir ve kullanılan metodun; ters saçılım problemlerinde önemli bir konu olan ve çok geniş kapsamlı pratik uygulamalara sahip tahribatsız muayene için etkili olduğu gösterilmiştir.

1. INTRODUCTION

Non-destructive testing (NDT) of materials is an important subject in the inverse scattering theory due to its wide range of practical applications such as but not limited to, automotive industry, medicine, aerospace engineering, construction etc. In a typical NDT problem the structure under test is excited by a certain type of field or wave and the reaction is measured on a region (usually non-contact to the structure) to extract the desired properties of the material under test. According to the physical configuration, number of methodologies has been developed such as magnetic particle method, eddy current method, ultrasonics, visual-optical methods, infrared thermography, acoustics, electromagnetics etc [1-5]. In electromagnetic applications microwave signals are capable of penetrating inside the dielectric media, allowing the inspection of the surfaces which are not reachable or not tend to be destructed to test. These applications are very important especially in the areas of detection of the mechanical damages, irregularities or cracks on coated surfaces of vehicles or on dielectric surfaces beyond layered media.

In imaging of an inaccessible surface one tries to recover the location and the shape as well as the surface characteristics of an unknown surface from scattered field measurements in a certain domain. The surface to be reconstructed can be either perfectly conducting or a dielectric interface. Several analytic and numerical techniques have been developed for perfectly conducting surfaces [6-12].

Most of the researches are based on the Kirchhoff approximation with the rough surface assumed to be locally planar [6, 9, 12]. In [6] the problem is reduced to the solution of two integral equations that can be solved approximately using a simple FFT-based approach. Another method using the Rytov approximation is used in [10]. In [11] the problem is reduced to the solution of a pair of coupled integral equations with two unknown functions in the case of grazing incidence.

Besides perfectly conducting interfaces, the reconstruction of a rough dielectric interface is a very important subject, because most of the boundaries in nature are in dielectric media. For the imaging of buried underground objects, the roughness of the

air–ground has to be known to simplify the problem. Some progress has been achieved in the solution of this problem [13, 14, 15]. The method presented in [15] uses both reflected and transmitted acoustic waves to reconstruct the surface using the Kirchhoff approximation and the method in [14] solves the profile estimation problem as a nonlinear optimization problem. In [13] a method based on merging a fast forward solver and an efficient optimization technique is presented using multi-incidence and multi-frequency reflected field measurements.

In this study; first, a method to determine the location and the shape of damages, irregularities, cracks, etc. on a dielectric rough surface located over a perfectly conducting plane is presented. For the sake of simplicity, surfaces having variation only in one space dimension are considered. A single illumination of plane electromagnetic wave with a fixed frequency is used for excitation and the scattered field measurements are performed on a line parallel to the boundary of the upper half space. The method is based on a special representation of the scattered field in each region where the Fourier transform and Taylor expansion are used together. By using the continuity conditions of the total field and its derivative on the interfaces, the problem is reduced to the solution of a coupled system of two integral equations with the unknowns; a spectral coefficient for the scattered field and interface function. The coupled system is solved iteratively by the use of classical Newton Method with the initial guess of the surface function. Fixing this surface function; one of the equations is solved to obtain the unknown spectral coefficient. Because of the ill-posedness, some regularization techniques are used. Then, fixing the spectral coefficient in the other equation, new surface function is obtained by linearization. Here, Newton Method and a regularization in least square sense is applied. The presented iterative method is tested by some numerical simulations and satisfactory results are obtained.

Second, the same method is applied for non-destructive testing of dielectric surfaces beyond a layered media. Results are obtained assuming the presence of two lossy dielectric media beyond the dielectric half space.

Throughout the paper, a time factor $\exp\{-i\omega t\}$ with frequency ω is assumed and omitted.

The organization of the paper is as follows: In Section 2, NDT of the dielectric rough surface located over a perfectly conducting plane is presented with numerical results. In Section 3, NDT of dielectric surfaces beyond a layered media is presented with numerical results. Conclusion is presented in Section 4.

2. NON-DESTRUCTIVE TESTING OF DIELECTRIC ROUGH SURFACE LOCATED OVER A PERFECTLY CONDUCTING PLANE

2.1 Representation of the scattered field

Consider the problem illustrated in Figure 2.1.

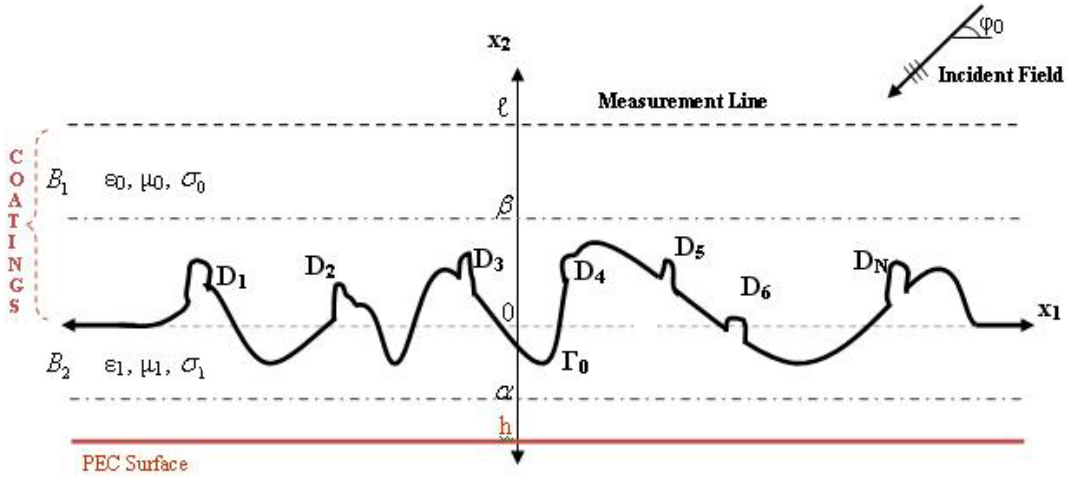

Figure 2.1 : Geometry of the problem

In this configuration Γ_0 is the destructed surface which is lying between two layers with electromagnetic parameters $\varepsilon_0, \mu_0, \sigma_0$ and $\varepsilon_1, \mu_1, \sigma_1$, respectively. The upper half space is assumed to be free space. The surface under test can be a flat or a rough one which is represented by a single-valued and continuous function $x_2 = f(x_1)$. Γ_0 is assumed to be locally rough, i.e.: $f(x_1)$ differs from zero over a finite interval which has a length of L_0. The main aim of the non-destructive testing problem considered here is to reconstruct the possible defects $D_1, D_2, \ldots$ on the surface through a set of scattered electromagnetic field measurements performed on the straight line $x_2 = l$ in the accessible region B_1. For the sake of simplicity, it will be assumed that the incident field is a TM polarized time-harmonic plane wave whose electric field vector is given by $\vec{E}^i = \left(0, 0, u^i(x_1, x_2)\right)$ with

$$u^i\left(x_1, x_2\right) = e^{-ik_0\left(x_1\cos\phi_0 + x_2\sin\phi_0\right)} \tag{2.1}$$

where ϕ_0 is the incident angle while $k_0 = \omega_0\sqrt{\varepsilon_0\mu_0}$. Due to the homogenity in the x_3 direction, the total and the scattered field vectors will have only x_3 components and the problem is reduced to a scalar one in terms of the total field function $u\left(x\right)$ which satisfies the Helmholtz equation

$$\Delta u + k^2 u = 0 \tag{2.2}$$

where,

$$k^2(x) = \begin{cases} {k_0}^2, & x_2 > f(x_1) \\ {k_1}^2, & h < x_2 < f(x_1) \end{cases} \tag{2.3}$$

In order to formulate the problem in an appropriate way, the total field is decomposed as:

$$u(x) = \begin{cases} u_1^s(x) + u^i(x), & x_2 > f(x_1) \\ u_2^s(x) + u_3^s(x), & h < x_2 < f(x_1) \end{cases} \tag{2.4}$$

where the functions u_1^s, u_2^s and u_3^s are the contributions of the defects and/or the roughness of the surface to the total field in the regions $x_2 > f\left(x_1\right)$ and $x_2 < f\left(x_1\right)$.

The boundary conditions imposed on the total field yield,

$$u_1^s + u^i = u_2^s + u_3^s \quad on\ x_2 = f\left(x_1\right) \tag{2.5}$$

$$\frac{\partial\left(u_1^s + u^i\right)}{\partial x_2} = \frac{\partial\left(u_2^s + u_3^s\right)}{\partial x_2} \ \text{on}\ x_2 = f\left(x_1\right) \tag{2.6}$$

$$u_2^s + u_3^s \quad \text{on}\ x_2 = h \tag{2.7}$$

$$\frac{\partial\left(u_2^s + u_3^s\right)}{\partial x_2} = 0 \ \text{on}\ x_2 = h \tag{2.8}$$

under the appropriate radiation condition for $x_2 \to \infty$.

In the following a special representation of the scattered field by the use of Fourier Transform and Taylor expansion is given. To this aim let us first define the Fourier Transform of u_1^s with respect to x_1 as:

$$\hat{u}_1^s(\nu, x_2) = \int_{-\infty}^{\infty} u_1^s(x_1, x_2) e^{-i\nu x_1} dx_1, \quad x_2 > \beta \tag{2.9}$$

where $\beta \geq \max\left(f\left(x_1\right)\right)$.

The Fourier transform of the reduced wave equation for u_1^s yields

$$\frac{d^2 \hat{u}_1^s}{dx_2^{\,2}} - \gamma_0 \hat{u}_1^s = 0, \quad x_2 > \beta \tag{2.10}$$

where $\gamma_0(\nu) = \sqrt{\nu^2 - k_0^2}$ is the square root function defined in the complex cut ν-plane as $\gamma_0(0) = -ik_0$. The solution of (2.9) can be given as

$$\hat{u}_1^s(\nu, x_2) = A(\nu) e^{-\gamma_0 x_2}, \quad x_2 > \beta \tag{2.11}$$

by taking the radiation condition into account. Here $A(\nu)$ is the unknown spectral coefficient. Then by applying the inverse Fourier Transform one can express u_1^s as

$$u_1^s\left(x\right) = \frac{1}{2\pi} \int_{-\infty}^{\infty} A\left(\nu\right) e^{i\nu x_1 - \gamma_0(\nu) x_2} d\nu, \quad x_2 > \beta \tag{2.12}$$

Now assume that the scattered field is measured on a line, which is parallel to the layers, in the upper half space i.e.; $u_1^s\left(x_1, l\right)$, $l > h$ is known for all $x_1 \in R$. Inserting $x_2 = l$ into (2.11); it is observed that, the spectral coefficient $A(\nu)$ can be determined from the Fourier transform via

$$A\left(\nu\right) = \hat{u}_1^s\left(\nu, \ell\right) e^{\gamma_0(\nu)\ell} \tag{2.13}$$

The same procedure can be easily applied for the scattered fields in the region $h < x_2 < \alpha$, in which $\alpha \le \min\left(f\left(x_1\right)\right)$, (see Figure 2.1) where there is no discontinuity in the x_1-direction. Thus,

$$u_2^s\left(x\right) = \frac{1}{2\pi}\int_{-\infty}^{\infty}\left(B\left(\nu\right)e^{\gamma_1(\nu)x_2} + C\left(\nu\right)e^{-\gamma_1(\nu)x_2}\right)e^{i\nu x_1}d\nu, \quad h < x_2 < \alpha \tag{2.14}$$

where $\gamma_1(\nu) = \sqrt{\nu^2 - k_1^2}$ with $\gamma_1(0) = -ik_1$ while $B\left(\nu\right), C\left(\nu\right)$ are the spectral coefficients to be determined.

Using the boundary conditions given in (2.7) and (2.8), $C\left(\nu\right)$ can be determined as

$$C\left(\nu\right) = -B\left(\nu\right)e^{2\gamma_1(\nu)h} \tag{2.15}$$

Substituting this equation in (2.14), the scattered field can be obtained as

$$u_2^s\left(x\right) = \frac{1}{2\pi}\int_{-\infty}^{\infty}B\left(\nu\right)\left(e^{\gamma_1(\nu)x_2} - e^{-\gamma_1(\nu)x_2}e^{2\gamma_1(\nu)h}\right)e^{i\nu x_1}d\nu, \quad h < x_2 < \alpha \tag{2.16}$$

To be able to find approximate expressions for the scattered field in the regions $x_2 \in \left(f\left(x_1\right), \beta\right)$ and $x_2 \in \left(\alpha, f\left(x_1\right)\right)$, Taylor expansions of the scattered field are used:

$$u_1^s\left(x\right) = \sum_{m=0}^{M}\frac{1}{m!}\frac{\partial^m u_1^s\left(x_1,\beta\right)}{\partial x_2^m}\left(x_2 - \beta\right)^m + R_m\left(x\right), \quad f\left(x_1\right) < x_2 \le \beta \tag{2.17}$$

$$u_2^s\left(x\right) = \sum_{m=0}^{N}\frac{1}{m!}\frac{\partial^m u_2^s\left(x_1,\alpha\right)}{\partial x_2^m}\left(x_2 - \alpha\right)^m + Q_N\left(x\right), \quad \alpha \le x_2 < f\left(x_1\right) \tag{2.18}$$

where the remainder terms are:

$$R_M\left(x\right) = \frac{1}{M!}\int_{\beta}^{x_2}\left(x_2 - \xi\right)^M\frac{\partial^{M+1}u_1^s\left(x_1,\xi\right)}{\partial x_2^{M+1}}d\xi \tag{2.19}$$

$$Q_N\left(x\right) = \frac{1}{N!}\int_{\alpha}^{x_2}\left(x_2 - \xi\right)^N\frac{\partial^{N+1}u_2^s\left(x_1,\xi\right)}{\partial x_2^{N+1}}d\xi \tag{2.20}$$

The m th order derivatives appearing in (2.17) and (2.18) can be obtained in the form of

$$\frac{\partial^m u_1^s(x_1,\beta)}{\partial x_2^m} = \frac{1}{2\pi}\int_{-\infty}^{\infty} A(\nu)[-\gamma_0(\nu)]^m e^{-\gamma_0(\nu)\beta}\, e^{i\nu x_1} d\nu \tag{2.21}$$

$$\frac{\partial^m u_2^s(x_1,\alpha)}{\partial x_2^m} = \frac{1}{2\pi}\int_{-\infty}^{\infty} B(\nu)\left(\left[\gamma_1(\nu)\right]^m e^{\gamma_1(\nu)\alpha} - \left[-\gamma_1(\nu)\right]^m e^{-\gamma_1(\nu)\alpha} e^{2\gamma_1(\nu)h}\right) e^{i\nu x_1} d\nu \tag{2.22}$$

By substituting the pairs (2.17) and (2.18) into the boundary conditions (2.5) and (2.6) and by neglecting the remainder terms:

$$\frac{1}{2\pi}\int_{-\infty}^{\infty}\left(B(\nu)\Psi_1(f)(x_1,\nu) - A(\nu)\Phi_1(f)(x_1,\nu)\right)e^{i\nu x_1} d\nu = r_1(f)(x_1) \tag{2.23}$$

$$\frac{1}{2\pi}\int_{-\infty}^{\infty}\left(B(\nu)\Psi_2(f)(x_1,\nu) - A(\nu)\Phi_2(f)(x_1,\nu)\right)e^{i\nu x_1} d\nu = r_2(f)(x_1) \tag{2.24}$$

can be obtained where

$$\Phi_1(f)(x_1,\nu) = e^{-\gamma_0(\nu)\beta}\sum_{m=0}^{M}\frac{[-\gamma_0(\nu)]^m}{m!}\left(f(x_1)-\beta\right)^m, \tag{2.25}$$

$$\Phi_2(f)(x_1,\nu) = e^{-\gamma_0(\nu)\beta}\sum_{m=1}^{M}\frac{[-\gamma_0(\nu)]^m}{(m-1)!}\left(f(x_1)-\beta\right)^{m-1}, \tag{2.26}$$

$$\Psi_1(f)(x_1,\nu) = \sum_{m=0}^{M}\frac{e^{\gamma_1(\nu)\alpha}[\gamma_1(\nu)]^m - e^{-\gamma_1(\nu)\alpha}[-\gamma_1(\nu)]^m}{m!}\left(f(x_1)-\alpha\right)^m, \tag{2.27}$$

$$\Psi_2(f)(x_1,\nu) = \sum_{m=1}^{M}\frac{e^{\gamma_1(\nu)\alpha}[\gamma_1(\nu)]^m - e^{-\gamma_1(\nu)\alpha}[-\gamma_1(\nu)]^m}{(m-1)!}\left(f(x_1)-\beta\right)^{m-1}, \tag{2.28}$$

and

$$r_1(f)(x_1) = u^i(x_1)\big|_{x_2=f(x_1)} = \mathrm{e}^{-ik_1\left(x_1\cos\phi_0 + f(x_1)\sin\phi_0\right)} \tag{2.29}$$

$$r_2(f)(x_1) = \left.\frac{\partial u^i(x_1)}{\partial x_2}\right|_{x_2=f(x_1)} = -ik_1 \sin\phi_0 \, e^{-ik_1(x_1\cos\phi_0 + f(x_1)\sin\phi_0)} \tag{2.30}$$

A more compact expression for the system above is given by the following operator equations:

$$K_1(f,B) - L_1(f,A) = r_1(f) \tag{2.31}$$

$$K_2(f,B) - L_2(f,A) = r_2(f) \tag{2.32}$$

In (2.31) and (2.32) K_1 and K_2 are non-linear operators with respect to $f(x_1)$ while they are linear with respect to $B(\nu)$. $A(\nu)$ values are calculated using (2.13).

2.2 Iterative Solution

The problem is reduced to the solution of this non-linear system given in (2.31) and (2.32) which can be treated by iterative techniques. First, an initial guess for the unknown surface variation f is chosen. Using this initial guess it is now easy to solve one of the equations, lets say (2.31), to obtain the spectral coefficient $B(\nu)$. Equation (2.31) becomes a linear function of $B(\nu)$, that is

$$K_1(B) = L_1 + r_1 \tag{2.33}$$

Here $K_1(B) = K_1(f,B)$ and $L_1 + r_1 = L_1(f,A) + r_1(f)$. Note that since both integral equations given by (2.31) and (2.32) are of the first kind one has to apply some regularization techniques. Here Tikhonov regularization is applied to obtain $B(\nu)$.

Tikhonov regularization, is one of the regularization methods used in ill-posed problems that solves the equation

$$Ax = b \tag{2.34}$$

using the Tikhonov matrix Γ, which is usually chosen as identity matrix I. Improving the conditioning of the problem the solution can be obtained as:

$$x = \left(A^T A + \Gamma^T \Gamma \right)^{-1} A^T b \tag{2.35}$$

In this work Tikhonov regularization is used with where $\Gamma = \alpha I$, where I is the identity matrix and α is the regularization parameter. Changing α, controls the effect of regularization and for an interval of α, it is possible to get satisfactory results of the unknown x.

Briefly, $B(v)$ can be obtained approximately which can be given as:

$$B = \left[\alpha_t I + K_1^* K_1 \right]^{-1} K_1 r \tag{2.36}$$

Once the unknown spectral coefficient is obtained approximately from (2.33), surface variation f can be obtained by using the other non-linear equation, (2.32) which can also be written in an operator form,

$$F_M(f) = K_2(B, f) - r_2(f) = 0. \tag{2.37}$$

(2.37) can be solved iteratively via Newton method. To this aim, for an initial guess f_0, the nonlinear equation is replaced by the linearized one

$$F_M(f_0) + F_M'(f_0)\Delta f = 0 \tag{2.38}$$

that needs to be solved for $\Delta f = f - f_0$ in order to improve an approximate boundary Γ_0 given by the function f_0 into a new approximation with surface function $f_0 + \Delta f$. The Newton method consists in iterating this procedure, i.e.: in solving

$$F_M'(f_0)\Delta f = -F_M(f_0), \quad i = 0,1,2,3,.... \tag{2.39}$$

for $\Delta f_{i+1} = f_i + \Delta f_{i+1}$. It is obvious that this solution will be sensitive to errors in the derivative of F_M in the vicinity of zeros. To obtain a more stable solution, the unknown Δf is expressed in terms of some basis functions $\phi_n(x_1), n = 1,...,N$, as a linear combination

$$\Delta f\left(x_1\right)=\sum_{n=1}^{N} a_n \phi_n\left(x_1\right). \tag{2.40}$$

A possible choice of basis functions consists of trigonometric polynomials. Then (2.39) is satisfied in the least squares sense, that is, the coefficients $a_1,...,a_N$ in (2.40) are determined such that for a set of grid points $x_1^1,...,x_1^J$ the sum of squares

$$\sum_{j=1}^{J}\left|F_M'\left(f\left(x_1^j\right)\right)\sum_{n=1}^{N} a_n \phi_n\left(x_1^j\right)+F_M\left(f\left(x_1^j\right)\right)\right|^2 \tag{2.41}$$

is minimized. The number of basis functions N in (2.40) can also be considered as a kind of regularization parameter. Choosing N too big leads to instabilities due to the ill-posedness of the inverse problem and too small values of N results in poor approximation quality.

2.3 Numerical Results

In this section some numerical results which demonstrate the validity and effectiveness of the method will be presented. In all the examples the upper space where the sources and observation points are located is assumed to be free-space. and the operating frequency is chosen as 12 GHz and the height of the measurement line is 5λ where λ is the free-space wavelength. The scattered data which should be collected by real measurements are computed synthetically by solving the associated direct problem for locally rough surfaces with a length of locality $L_0=10\lambda$. The data are sampled on the measurement line in an interval $\left[-20\lambda,20\lambda\right]$ and 1% random noise is added to the simulated data for the scattered field. In the application of least squares solution the basis functions are chosen as combinations of $\cos\left(2\pi n x_1/L_0\right)$ and $\sin\left(2\pi n x_1/L_0\right)$, $n=0,\pm1,...\pm N,$ and the number N is determined by trial and error. As it can be observed from Figure 2.2 and Figure 2.3, the method is very effective for defects having sizes in order of $\lambda/200$ for planar and curved surfaces.

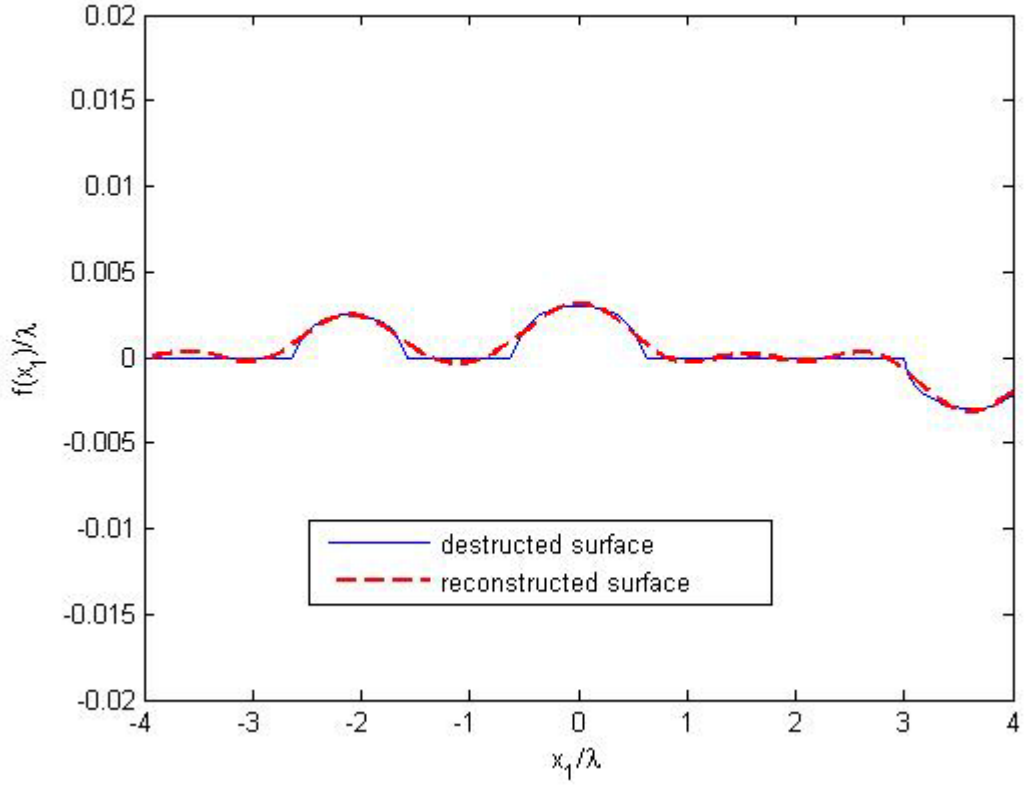

Figure 2.2 : Reconstruction of defects on planar surface

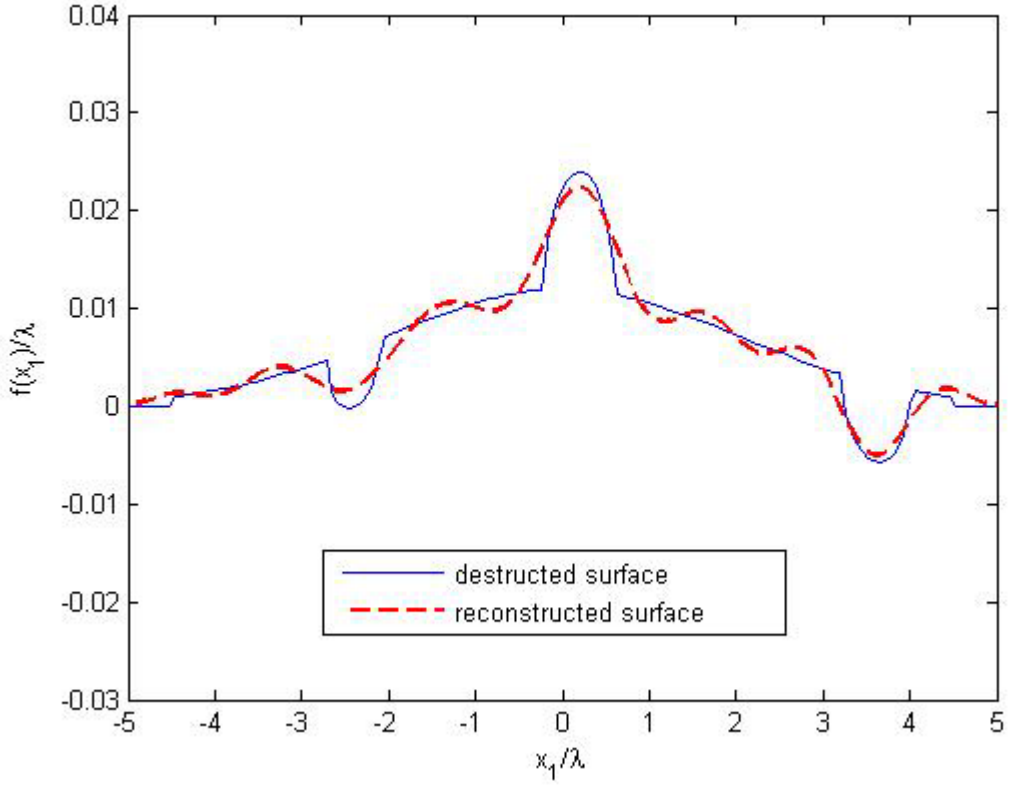

Figure 2.3 : Reconstruction of defects on curved surface

2.4 Parameters Affecting Reconstruction

2.4.1 Number of Iterations

Consider the case in which the relative dielectric permittivity of the second layer is selected as $\varepsilon_1 = 5\varepsilon_0$ and the conductivity of the second layer is selected as 0.0001 S/m. The reconstruction of the circular defects on a planar surface shown in Figure 2.4 is obtained for the truncation number $M = 3$ in the Taylor expansion for 1 and 3 iterations. Tikhonov regularization parameter is selected as 0.001 and least square regularization parameter is selected as $N = 8$. After 3 iterations, it is possible to have satisfactory results for the surface.

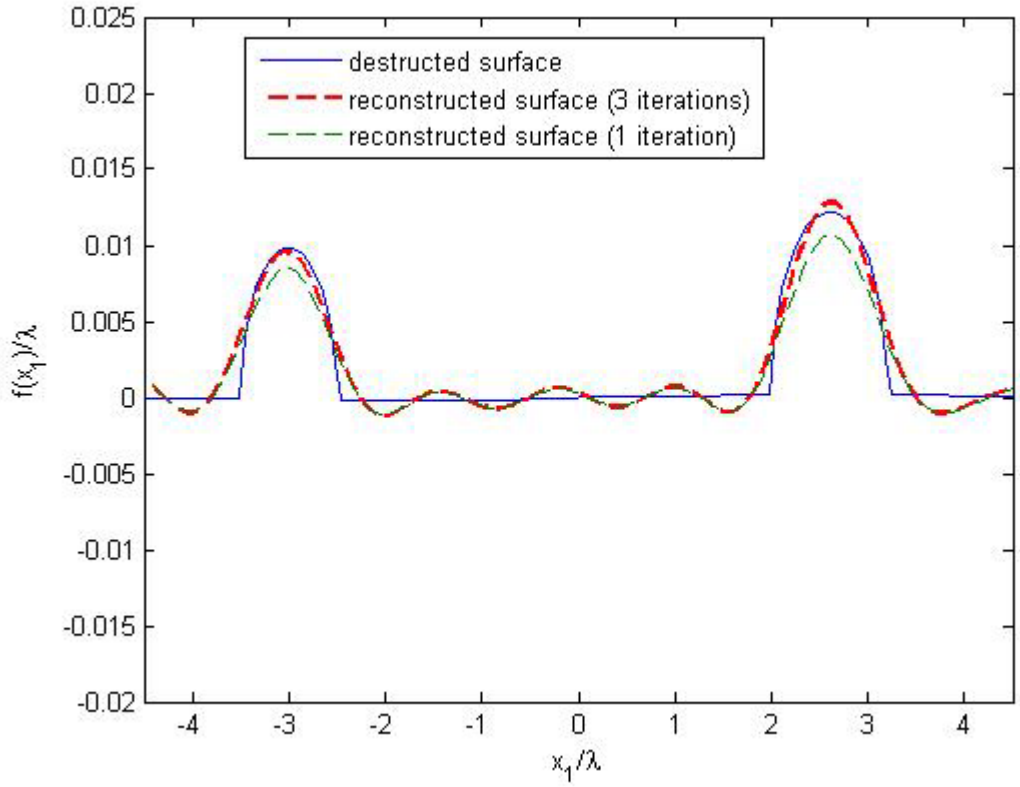

Figure 2.4 : Destructed and reconstructed surfaces

2.4.2 Truncation Number

The dielectric surface is located above a non-magnetic painting material having electromagnetic parameters $\varepsilon_2 = 4\varepsilon_0$, $\sigma_2 = 10^{-4}$ and below a non-magnetic painting material having electromagnetic parameters $\varepsilon_1 = \varepsilon_0$, $\sigma_1 = 0$. On the surface shown in Figure 2.5, reconstruction of the defects is obtained for the truncation number

$M = 2$, $M = 3$ and $M = 6$ in the Taylor expansion for 2 iterations. This simulation determines the accuracy of the reconstructed surface depending on the truncation number. And it can be seen that for $M = 2$, $M = 3$ and $M = 6$ results are nearly the same. As the surface gets wider, it is supposed to converge to the more accurate results as truncation number gets larger. But for this surface it is enough to select $M = 2$ or $M = 3$ in order to get good results.

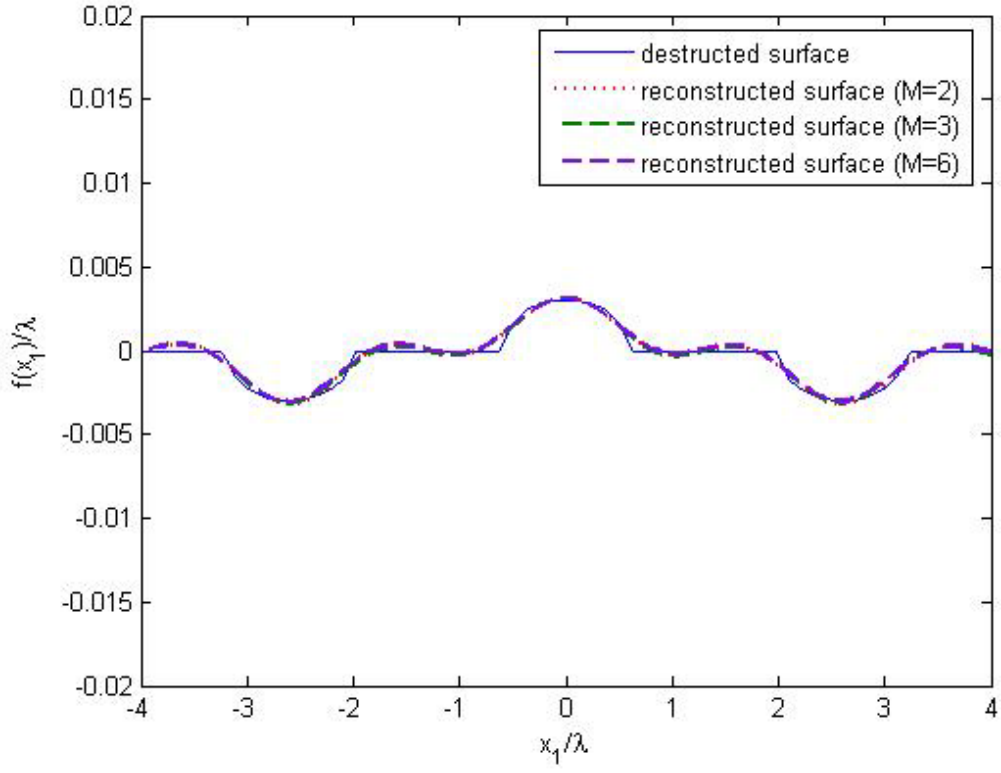

Figure 2.5 : Destructed and reconstructed surfaces for different truncation numbers

2.4.3 Regularization Parameter

In this simulation painting material below the surface to be reconstructed has the electromagnetic parameters $\varepsilon_2 = 4\varepsilon_0$, $\sigma_2 = 10^{-4}$ and above the surface $\varepsilon_1 = \varepsilon_0$, $\sigma_1 = 0$. In order to find the spectral coefficient Tikhonov regularization is applied with regularization parameter α, which is selected 0.000001, 0.001 and 0.05 with the truncation number of $M = 4$, for 3 iterations. The incident angle is assumed to be $\pi/2$. Figure 2.6 shows that reconstruction method results better with $\alpha = 0.000001$ for this example. Regularization parameter has to be selected from the interval $0 < \alpha < 1$.

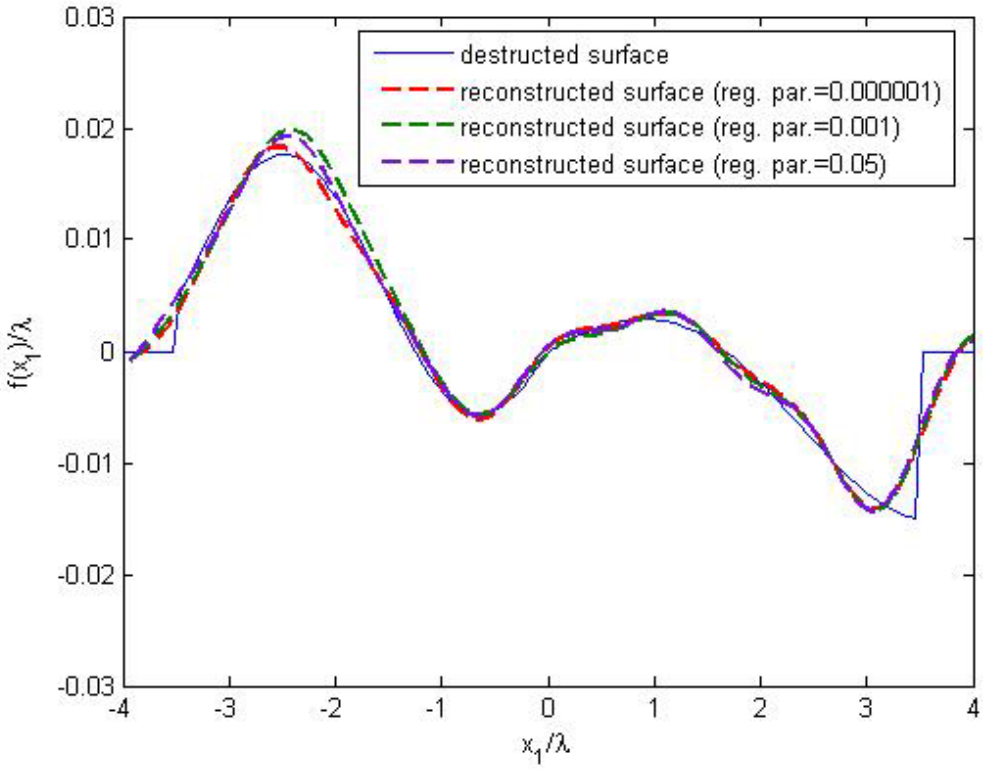

Figure 2.6 : Destructed and reconstructed surfaces for different regularization parameters

2.4.4 Incident Angle

In this example the dielectric surface is located above a non-magnetic painting material having electromagnetic parameters $\varepsilon_2 = 4\varepsilon_0$, $\sigma_2 = 10^{-4}$ and below a non-magnetic painting material having electromagnetic parameters $\varepsilon_1 = \varepsilon_0$, $\sigma_1 = 0$. The reconstruction of the circular defects on a rough surface shown in Figure 2.7 is obtained for the truncation number $M = 3$ in the Taylor expansion for 3 iterations. This simulation determines the accuracy of the reconstructed surface depending on the incident angle of $\pi/2,\ \pi/3,\ \pi/4$. The results show that reconstruction gets more accurate with the incident angles closer to $\pi/2$.

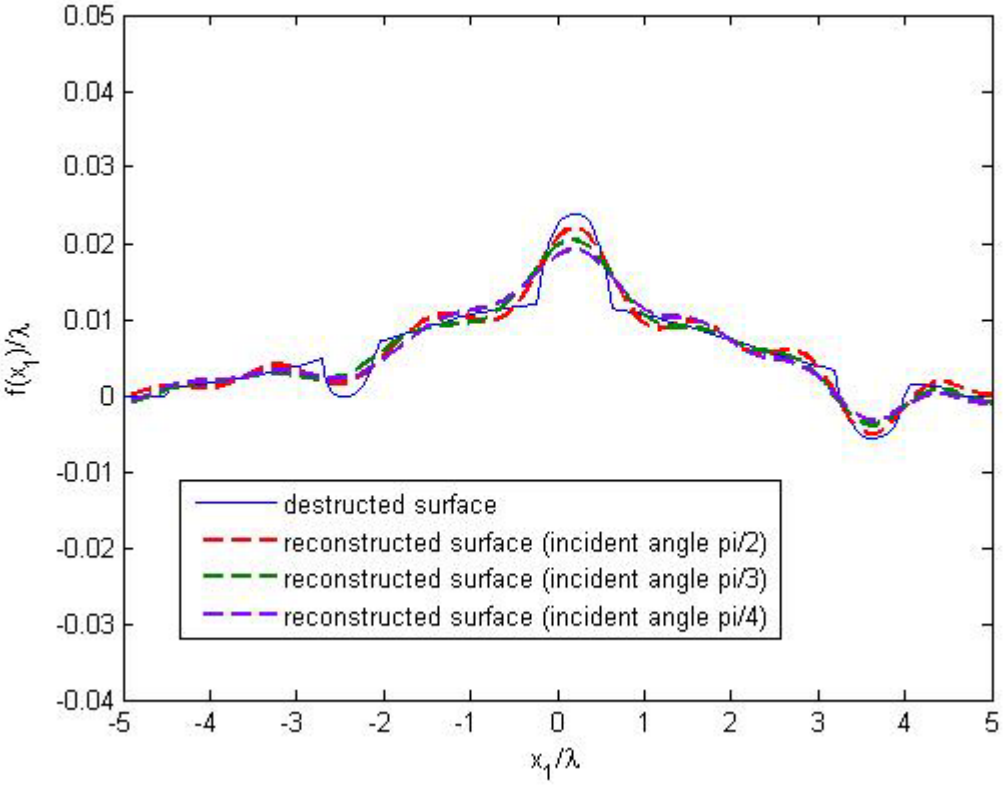

Figure 2.7 : Destructed and reconstructed surfaces for different incidence directions

2.4.5 Noise Level

The simulation results given in Figure are obtained to test the accuracy of the method against different noise levels; 1% and 5% with the truncation number $M = 3$, after 3 iterations. It can be seen that the method is robust against noise with different levels.

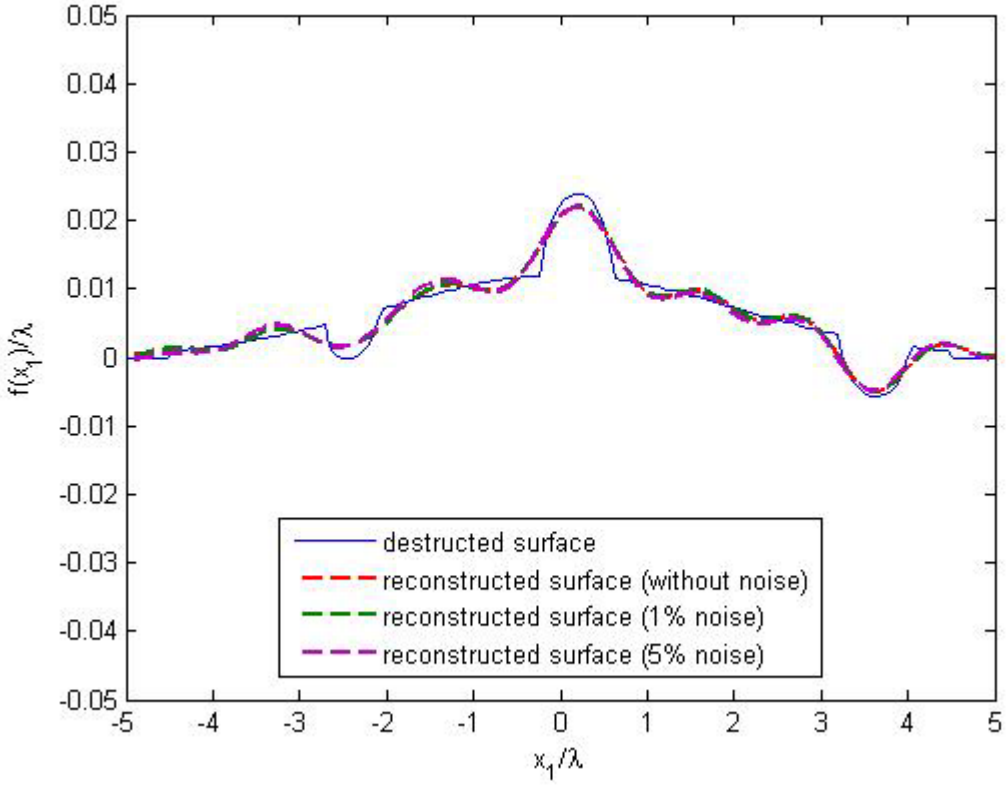

Figure 2.8 : Destructed and reconstructed surfaces for different noise levels

3. NON-DESTRUCTIVE TESTING OF DIELECTRIC SURFACES BEYOND A LAYERED MEDIA

3.1 Representation of the scattered field

Consider the problem illustrated in Figure 3.1.

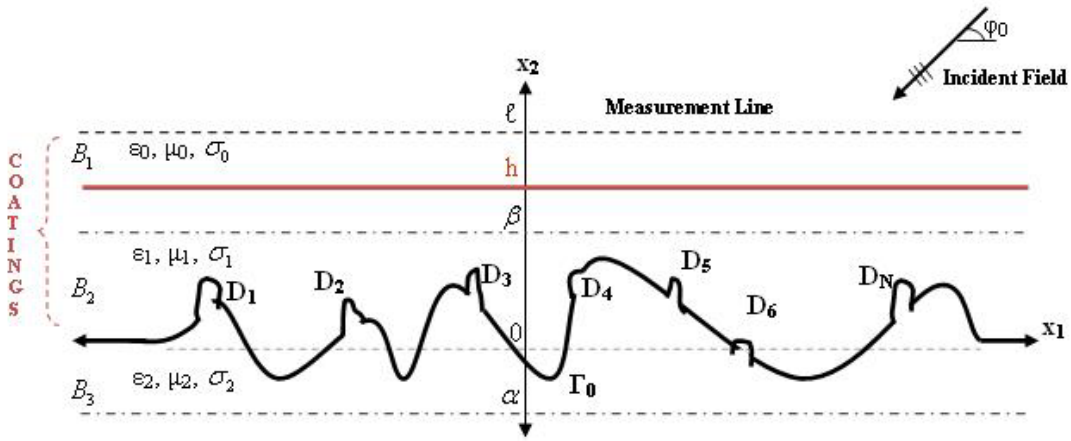

Figure 3.1 : Geometry of the problem

Γ_0 is the destructed surface which is lying between two layers with electromagnetic parameters $\varepsilon_0, \mu_0, \sigma_0$ and $\varepsilon_1, \mu_1, \sigma_1$, respectively. The upper half space is assumed to be free space. The surface under test can be represented by $x_2 = f(x_1)$ which is assumed to be locally rough, It is aimed to reconstruct the possible defects $D_1, D_2, \ldots$ on the surface Γ_0 through a set of scattered electromagnetic field measurements performed in the accessible domain $x_2 > h$. Here h represents the boundary between the layers above the surface under test. The incident field is again assumed to be a TM polarized time-harmonic plane wave whose electric field vector is given by $\vec{E}^i = \left(0, 0, u^i(x_1, x_2)\right)$ with $u^i(x_1, x_2) = e^{-ik_0(x_1 \cos\phi_0 + x_2 \sin\phi_0)}$ where ϕ_0 is the incident angle while $k_0 = \omega_0 \sqrt{\varepsilon_0 \mu_0}$.

Total field function $u(x)$ satisfies the Helmholtz equation

$$\Delta u + k^2 u = 0 \tag{3.1}$$

where,

$$k^2(x) = \begin{cases} {k_0}^2, & x_2 > h \\ {k_1}^2, & h > x_2 > f(x_1) \\ {k_2}^2, & x_2 > f(x_1) \end{cases} \tag{3.2}$$

The total field can be shown as

$$u(x) = \begin{cases} u_1^s(x) + u^i(x), & x_2 > h \\ u_2^s(x), & h > x_2 > f(x_1) \\ u_3^s(x), & x_2 < f(x_1) \end{cases} \tag{3.3}$$

where the functions u_1^s, u_2^s and u_3^s are the contributions of the defects and/or the roughness of the surface to the total field in the regions $x_2 > h$, $x_2 \in \left(f(x_1), h\right)$ and $x_2 < f(x_1)$ respectively.

The boundary conditions can be written as,

$$u_1^s + u^i = u_2^s \quad \text{on } x_2 = h \tag{3.4}$$

$$\frac{\partial\left(u_1^s + u^i\right)}{\partial x_2} = \frac{\partial u_2^s}{\partial x_2} \quad \text{on } x_2 = h \tag{3.5}$$

$$u_2^s = u_3^s \quad \text{on } x_2 = f(x_1) \tag{3.6}$$

$$\frac{\partial u_2^s}{\partial x_2} = \frac{\partial u_3^s}{\partial x_2} \quad \text{on } x_2 = f(x_1) \tag{3.7}$$

under the appropriate radiation condition for $x_2 \to \infty$.

Fourier Transform of u_1^s can be given as:

$$\hat{u}_1^s(\nu, x_2) = \int_{-\infty}^{\infty} u^s(x_1, x_2) e^{-i\nu x_1} dx_1, \quad x_2 > h \tag{3.8}$$

The Fourier transform of the reduced wave equation for u_1^s yields

$$\frac{d^2\hat{u}_1^s}{dx_2^{\,2}} - \gamma_0 \hat{u}_1^s = 0, \quad x_2 > h \tag{3.9}$$

where $\gamma_0(\nu) = \sqrt{\nu^2 - k_0^2}$ is the square root function defined in the complex cut ν-plane as $\gamma_0(0) = -ik_0$. The solution of (3.8) can be given as

$$\hat{u}_1^s(\nu, x_2) = A(\nu) e^{-\gamma_0 x_2}, \quad x_2 > h \tag{3.10}$$

by taking the radiation condition into account where $A(\nu)$ is the unknown spectral coefficient. u_1^s can be written as

$$u_1^s(x) = \frac{1}{2\pi} \int_{-\infty}^{\infty} A(\nu) e^{i\nu x_1 - \gamma_0(\nu) x_2} d\nu, \quad x_2 > h \tag{3.11}$$

by applying the inverse Fourier Transform.

The same procedure can be applied for the scattered fields in the regions $x_2 \in (\beta, h)$ and $x_2 < \alpha$, where $\beta \geq \max\left(f(x_1)\right)$ and $\alpha \leq \min\left(f(x_1)\right)$ (see Figure 3.1). In these regions there is no discontinuity in the x_1-direction.

Scattered fields can be represented as:

$$u_2^s(x) = \frac{1}{2\pi} \int_{-\infty}^{\infty} \left(B(\nu) e^{-\gamma_1(\nu) x_2} + C(\nu) e^{\gamma_1(\nu) x_2} \right) e^{i\nu x_1} d\nu, \quad \beta < x_2 < h \tag{3.12}$$

$$u_3^s(x) = \frac{1}{2\pi} \int_{-\infty}^{\infty} D(\nu) e^{i\nu x_1 + \gamma_2(\nu) x_2} d\nu, \quad x_2 < \alpha \tag{3.13}$$

where $\gamma_1(\nu) = \sqrt{\nu^2 - k_1^2}$ and $\gamma_2(\nu) = \sqrt{\nu^2 - k_2^2}$ with $\gamma_1(0) = -ik_1$ and $\gamma_2(0) = -ik_2$ while $B(\nu), C(\nu)$ and $D(\nu)$ are the spectral coefficients to be determined.

Now assume that the scattered field is measured on a line, which is parallel to the layers, in the upper half space i.e.; $u_1^s(x_1, l)$, $l > h$ is known for all $x_1 \in R$. Inserting

$x_2 = l$ into (3.10), the spectral coefficient $A(\nu)$ can be determined from the Fourier transform as;

$$A(\nu) = \hat{u}_1^s(\nu, \ell)\, e^{\gamma_0(\nu)\ell}. \tag{3.14}$$

Using boundary conditions (3.4) and (3.5) on $x_2 = h$, the unknown spectral coefficients $B(\nu)$ and $C(\nu)$ can be obtained.

$$u_i(x_1, h) + u_1^s(x_1, h) = \frac{1}{2\pi}\int_{-\infty}^{\infty}\left(B(\nu)e^{-\gamma_1(\nu)h} + C(\nu)e^{\gamma_1(\nu)h}\right)e^{i\nu x_1}d\nu \tag{3.15}$$

$$\left.\frac{\partial u_1^s(x_1,x_2)}{\partial x_2}\right|_{x_2=h} + \left.\frac{\partial u_i(x_1,x_2)}{\partial x_2}\right|_{x_2=h} = \frac{1}{2\pi}\int_{-\infty}^{\infty}\left(B(\nu)\left(-\gamma_1(\nu)\right)e^{-\gamma_1(\nu)h} + C(\nu)\left(\gamma_1(\nu)\right)e^{\gamma_1(\nu)h}\right)e^{i\nu x_1}d\nu. \tag{3.16}$$

By discretizing the equations (3.15) and (3.16) and using Tikhonov regularization, $B(\nu)$ and $C(\nu)$ can be obtained.

To be able to find approximate expressions for the scattered field in the regions $x_2 \in (f(x_1), \beta)$ and $x_2 \in (\alpha, f(x_1))$ where there are discontinuities in the x_1-direction, Taylor expansions of the scattered field are used:

$$u_2^s(x) = \sum_{m=0}^{M}\frac{1}{m!}\frac{\partial^m u_2^s(x_1,\beta)}{\partial x_2^m}(x_2-\beta)^m + R_m(x), \quad f(x_1) < x_2 \le \beta \tag{3.17}$$

$$u_3^s(x) = \sum_{m=0}^{N}\frac{1}{m!}\frac{\partial^m u_3^s(x_1,\alpha)}{\partial x_2^m}(x_2-\alpha)^m + Q_N(x), \quad \alpha \le x_2 < f(x_1) \tag{3.18}$$

where the remainder terms are:

$$R_M(x) = \frac{1}{M!}\int_{\beta}^{x_2}(x_2-\xi)^M\frac{\partial^{M+1}u_2^s(x_1,\xi)}{\partial x_2^{M+1}}d\xi \tag{3.19}$$

$$Q_N(x) = \frac{1}{N!}\int_{\alpha}^{x_2}(x_2-\xi)^N\frac{\partial^{N+1}u_3^s(x_1,\xi)}{\partial x_2^{N+1}}d\xi \tag{3.20}$$

The m th order derivatives used in (3.17) and (3.18) can be written in the form of

$$\frac{\partial^m u_2^s(x_1,\beta)}{\partial x_2^m}=\frac{1}{2\pi}\int_{-\infty}^{\infty}\left([-\gamma_1(\nu)]^m B(\nu)e^{-\gamma_1(\nu)\beta}+[\gamma_1(\nu)]^m C(\nu)e^{\gamma_1(\nu)\beta}\right)e^{i\nu x_1}d\nu \tag{3.21}$$

$$\frac{\partial^m u_3^s(x_1,\alpha)}{\partial x_2^m}=\frac{1}{2\pi}\int_{-\infty}^{\infty}\left([\gamma_2(\nu)]^m D(\nu)e^{\gamma_2(\nu)\alpha}\right)e^{i\nu x_1}d\nu. \tag{3.22}$$

Substituting the pairs (3.17) and (3.18) into the boundary conditions (3.6) and (3.7) and neglecting the remainder terms,

$$\frac{1}{2\pi}\int_{-\infty}^{\infty}D(\nu)\Phi_3(f)(x_1,\nu)e^{i\nu x_1}d\nu=\frac{1}{2\pi}\int_{-\infty}^{\infty}\left(B(\nu)\Phi_1(f)(x_1,\nu)+C(\nu)\Phi_2(f)(x_1,\nu)\right)e^{i\nu x_1}d\nu \tag{3.23}$$

$$\frac{1}{2\pi}\int_{-\infty}^{\infty}D(\nu)\Psi_3(f)(x_1,\nu)e^{i\nu x_1}d\nu=\frac{1}{2\pi}\int_{-\infty}^{\infty}\left(B(\nu)\Psi_1(f)(x_1,\nu)+C(\nu)\Psi_2(f)(x_1,\nu)\right)e^{i\nu x_1}d\nu \tag{3.24}$$

can be obtained where

$$\Phi_1(f)(x_1,\nu)=e^{-\gamma_1(\nu)\beta}\sum_{m=0}^{M}\frac{[-\gamma_1(\nu)]^m}{m!}\left(f(x_1)-\beta\right)^m, \tag{3.25}$$

$$\Psi_1(f)(x_1,\nu)=e^{-\gamma_1(\nu)\beta}\sum_{m=1}^{M}\frac{[-\gamma_1(\nu)]^m}{(m-1)!}\left(f(x_1)-\beta\right)^{m-1}, \tag{3.26}$$

$$\Phi_2(f)(x_1,\nu)=e^{\gamma_1(\nu)\beta}\sum_{m=0}^{M}\frac{[\gamma_1(\nu)]^m}{m!}\left(f(x_1)-\beta\right)^m, \tag{3.27}$$

$$\Psi_2(f)(x_1,\nu)=e^{\gamma_1(\nu)\beta}\sum_{m=1}^{M}\frac{[\gamma_1(\nu)]^m}{(m-1)!}\left(f(x_1)-\beta\right)^{m-1}, \tag{3.28}$$

$$\Phi_3(f)(x_1,\nu)=e^{\gamma_2(\nu)\alpha}\sum_{m=0}^{N}\frac{[\gamma_2(\nu)]^m}{m!}\left(f(x_1)-\alpha\right)^m, \tag{3.29}$$

$$\Psi_3(f)(x_1,\nu)=e^{\gamma_2(\nu)\beta}\sum_{m=1}^{M}\frac{[\gamma_2(\nu)]^m}{(m-1)!}\left(f(x_1)-\alpha\right)^{m-1}. \tag{3.30}$$

The problem is reduced to a system of nonlinear equations including the spectral coefficient $D(\nu)$ related to the scattered field u_3^s and the variation of the rough surface $f(x_1)$.

A more compact expression for the system is given by the following operator equations:

$$K_1\left(D(\nu), f\right) = g_1\left(f\right) \tag{3.31}$$

$$K_2\left(D(\nu), f\right) = g_2\left(f\right) \tag{3.32}$$

In (3.31) and (3.32) K_1 and K_2 are non-linear operators with respect to $f(x_1)$ while they are linear with respect to $D(\nu)$.

3.2 Iterative Solution

The solution of this non-linear system which can be solved by iterative techniques. First an initial guess for the unknown surface variation f ıs chosen. Using this initial guess one of the equations mentioned above ıs solved to obtain the spectral coefficient $D(\nu)$ by applyıng some regularization techniques. Here again Tikhonov regularization is applied. Once the unknown spectral coefficient ıs obtaıned from one of the equations, say the first one; surface variation f can be obtained by solving the other non-linear equation, which can also be written in an operator form,

$$F_M\left(f\right) = K_2\left(D, f\right) - g_2\left(f\right) = 0 \tag{3.33}$$

which can be solved iteratively via Newton method explained in the previous section. To get more stable solution, least square regularization can be applied again where the number of basis functions N can be considered as a kind of regularization parameter.

3.3 Numerical Results

In the first example, the dielectric surface is located above a non-magnetic painting material having electromagnetic parameters $\varepsilon_2 = 7\varepsilon_0$, $\sigma_2 = 10^{-4}$ and below a non-

magnetic painting material having electromagnetic parameters $\varepsilon_2 = 4\varepsilon_0$, $\sigma_2 = 10^{-4}$. The reconstruction of the circular defects on a planar surface shown in Figure 3.2 is obtained for the truncation number $M = 5$ in the Taylor expansion for 2 iterations. Regularization parameter is selected as 0.005. The method determines the locations and the shapes of the defects having depths in the order of $\lambda / 200$ very accurately. The results given in the Figure 3.3 shows that the method can be effectively used for reconstruction of the defects on curved surfaces. It shows the reconstruction obtained for the truncation numbers $M = 5$ with 3 iterations and the regularization parameter is selected 0.005.

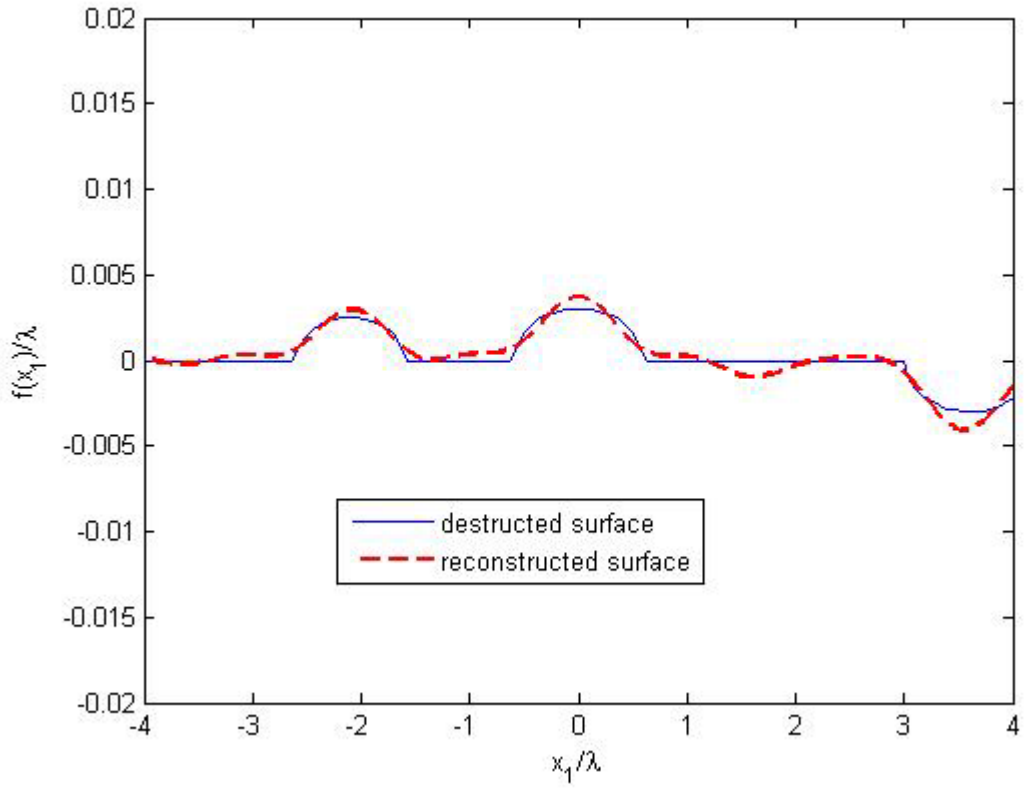

Figure 3.2 : Reconstruction of defects on planar surface

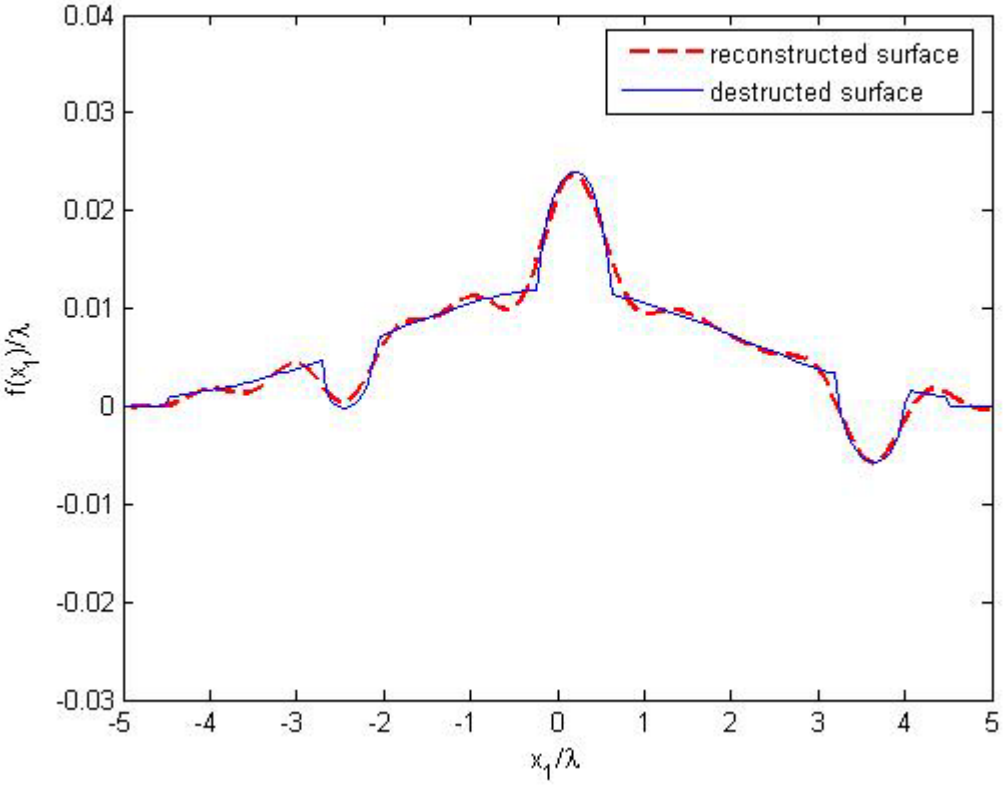

Figure 3.3 : Reconstruction of defects on curved surface

3.4 Parameters Affecting Reconstruction

3.4.1 Number of Iterations

In this simulation, destructed surface is located above a material having electromagnetic parameters $\varepsilon_2 = 7\varepsilon_0$, $\sigma_2 = 10^{-4}$ and below a material having electromagnetic parameters $\varepsilon_2 = 4\varepsilon_0$, $\sigma_2 = 10^{-4}$. The reconstruction given in Figure 3.4 is obtained for the truncation number $M = 3$ in the Taylor expansion for 1 and 3 iterations. Tikhonov regularization parameter is selected 0.001 and least square regularization parameter is selected as $N = 8$.

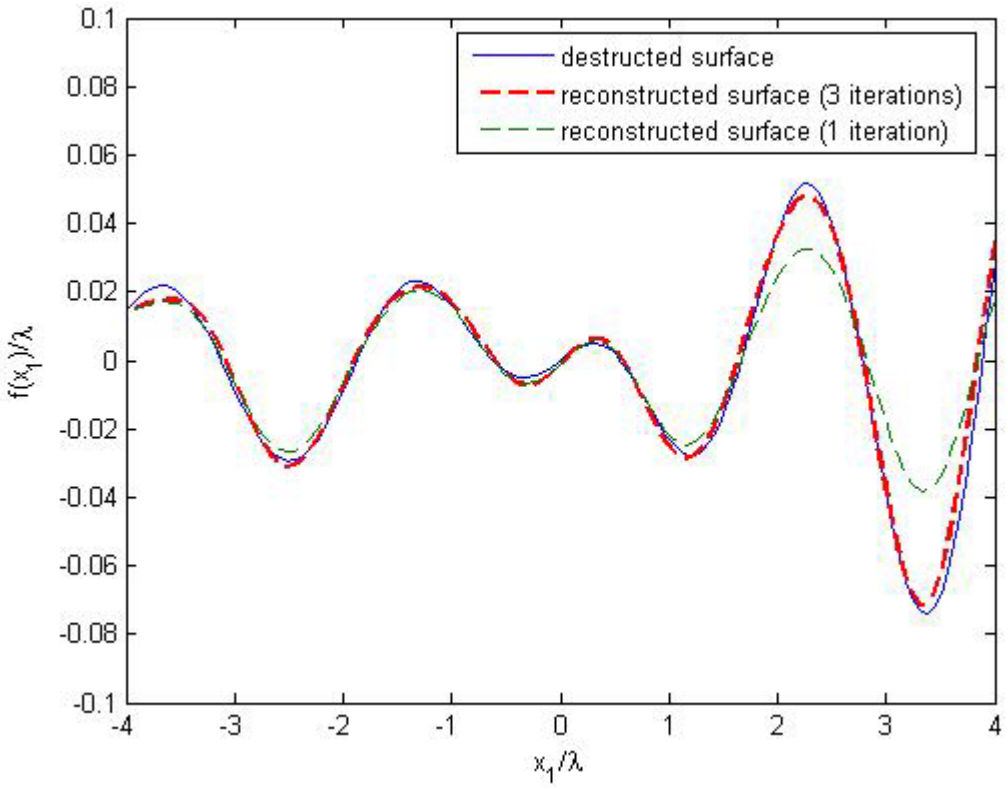

Figure 3.4 : Destructed and reconstructed surfaces

3.4.2 Truncation Number

For the same conditions, reconstruction of the defects is obtained for the truncation number $M = 2$, $M = 3$ and $M = 8$ in the Taylor expansion for 3 iterations. For $M = 2$, surface can not be reconstructed accurately while for $M = 3$ and $M = 8$, results are nearly the same which shows that it converges to the more accurate results as truncation number gets larger.

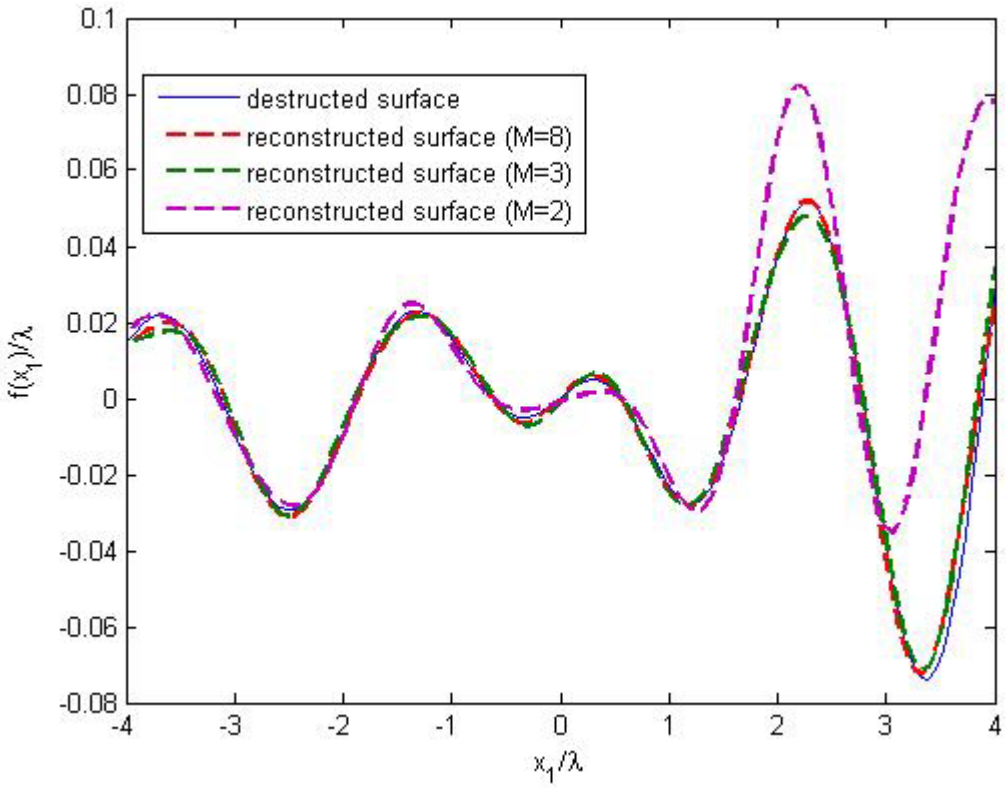

Figure 3.5 : Destructed and reconstructed surfaces for different truncation numbers

3.4.3 Regularization Parameter

In this simulation, the dielectric surface is located above a non-magnetic painting material having electromagnetic parameters $\varepsilon_2 = 7.5\varepsilon_0$, $\sigma_2 = 10^{-4}$ and below a material having electromagnetic parameters $\varepsilon_2 = 5\varepsilon_0$, $\sigma_2 = 10^{-4}$. The reconstruction of the circular defects on a rough surface shown in Figure 3.6 is obtained for the truncation number $M = 8$ in the Taylor expansion for 3 iterations and the incident angle is assumed to be $\pi/2$. Regularization parameters are selected as 0.000001, 0.001 and 0.05 in order to make comparison. Reconstruction method results better with $\alpha = 0.001$ and $\alpha = 0.05$ for this example. Regularization parameter has to be selected from the interval $0 < \alpha < 1$.

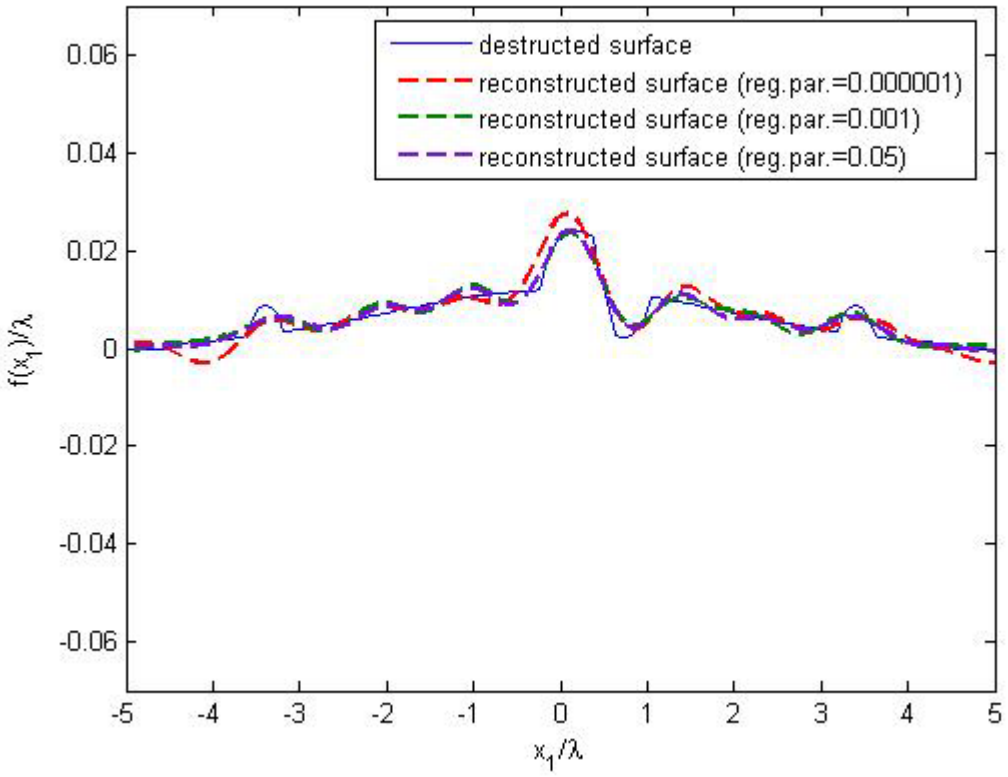

Figure 3.6 : Destructed and reconstructed surfaces for different regularization parameters

3.4.4 Incidence Angle

In this simulation destructed surface is located above a material having electromagnetic parameters $\varepsilon_2 = 7\varepsilon_0$, $\sigma_2 = 10^{-4}$ and below a material having electromagnetic parameters $\varepsilon_2 = 4\varepsilon_0$, $\sigma_2 = 10^{-4}$. The reconstruction of the circular defects on a rough surface shown in Figure 3.7 is obtained for the truncation number $M = 5$ in the Taylor expansion for 2 iterations. This simulation determines the accuracy of the reconstructed surface depending on the incident angle of $\pi/2,\ \pi/3,\ \pi/4$ which results better with the incident angles closer to $\pi/2$ like in the first case.

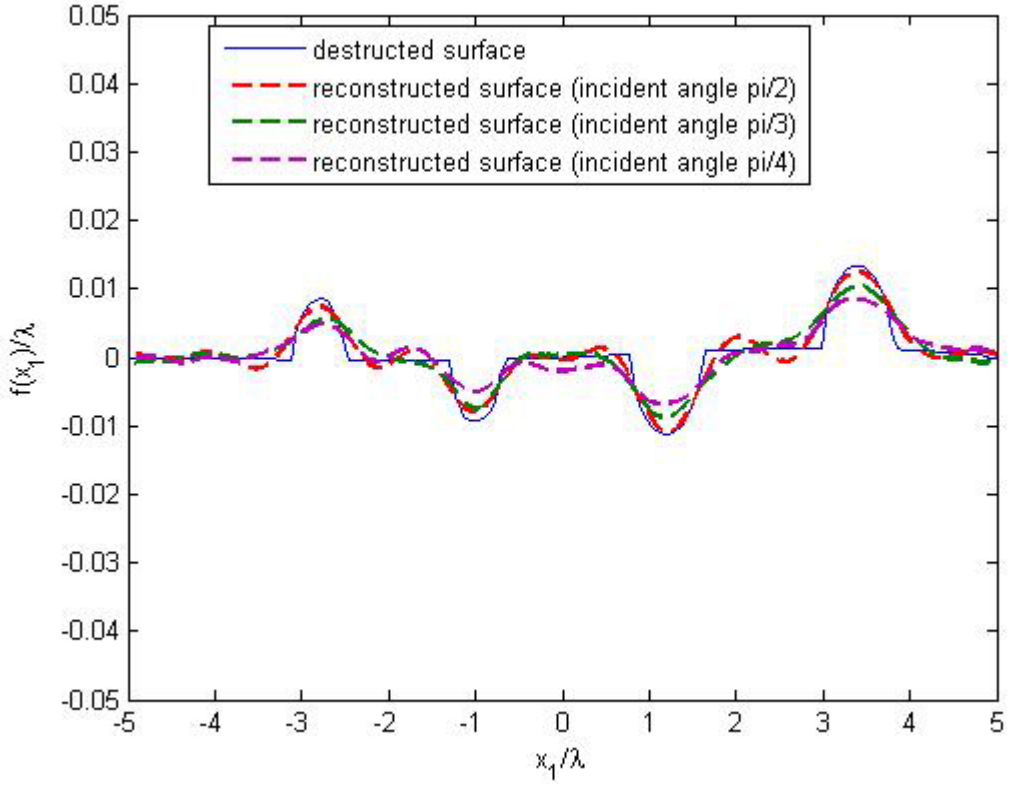

Figure 3.7 : Destructed and reconstructed surfaces for different incidence directions

3.4.5 Noise Level

Destructed interface is located above a material having electromagnetic parameters $\varepsilon_2 = 7\varepsilon_0$, $\sigma_2 = 10^{-4}$ and below a material having electromagnetic parameters $\varepsilon_2 = 4\varepsilon_0$, $\sigma_2 = 10^{-4}$. Regularization parameters are selected as 0.000001. In Figure 3.8 method is tested against different noise levels; 1% and 5% with the truncation number $M = 5$, after 2 iterations and it can be seen that method is robust against noise with different levels again.

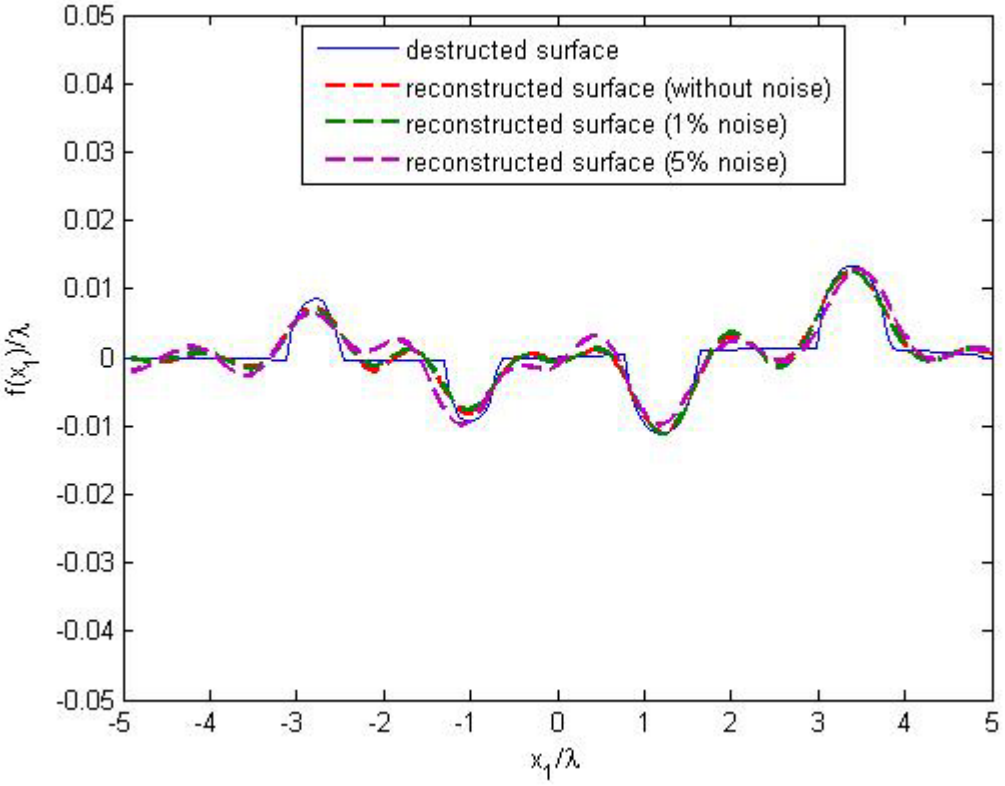

Figure 3.8 : Destructed and reconstructed surfaces for different noise level

4. CONCLUSION

In this study, the method presented in [17] is extended to the non-destructive evaluation of the dielectric surface above a perfectly conducting plane in the first case and beyond a layered media in the second case. The method is very effective for defects having sizes in order of $\lambda/200$ for an operating frequency of 12 GHz. From the simulation results, it is observed that the accurancy of reconstructions are closely related with the truncation number in Taylor expansion where using more terms in Taylor expansion results in higher resolution. Also, incident angle of the plane electromagnetic wave affects the simulations giving better results in normal incidence. The method is robust against different noise levels and 3 or more iterations are enough to obtain satisfactory results for the surfaces given in simulations.

REFERENCES

[1] **Mohammadi, J.,** 2004. Non-destructive Test (NDT) Methods Applied Fatigue Reliability Assessment of Structures ASCE Publications, Reston, VA, USA.

[2] **Ganchev, S. I., Qaddoumi, N., Ranu, E., Zoughi, R.,** 1995. Microwave detection optimization of disbond in layered dielectrics with varying thickness, *IEEE Transactions on Instrumentation and Measurement*, **44**, 326-328.

[3] **Nadakuduti, J., Chen, G., Zoughi, R.,** 2006. Semiempirical Electromagnetic Modeling of Crack Detection and Sizing in Cement-based Materials using Near-Field Microwave Methods, *IEEE Transactions on Instrumantation and Measurement*, **55**, 588-597.

[4] **Massa, A., Pastorino, M., Rosani, A., Benedetti, M.,** 2006. A Microwave Imaging Method for NDE/NDT based on the SMW Technique for the Electromagnetic Field Prediction, *IEEE Transactions on Instrumantation and Measurement*, **55**, 240-247.

[5] **Benedetti, M., Donelli, M., Martini, A., Pastorino, M., Rosani, A., Massa, A.,** 2006. An Innovative Microwave-Imaging Technique for Nondestructive Evaluation: Applications to Civil Structures monitoring and Biological Bodies Inspection, *IEEE Transactions on Instrumantation and Measurement*, **55**, 1878-1884.

[6] **Destouches, N., Guerin, C.A., Lequime, M., Giovannini H.,** 2001. Determination of the phase of the diffracted field in the optical domain: application to the reconstruction of surface profiles, *Optics Communications*, **198**, 233-239.

[7] **Harada, K., Nouchi A.,** 1996. Reconstruction of two-dimensional rough surface with Gaussian beam illuminations, *IEICE Transactions on Electronics*, **E79-C**, 1345-1349.

[8] **Jin, Y.Q. and Li, Z.,** 2001. Reconstruction of roughness profile of fractal surface from scattering measurements at grazing incidence, *Journal of Applied Physics*, **89**, 1922–1926.

[9] **Quartel, J.C., Sheppard, C.J.R.,** 1996. Surface reconstruction using an algorithm based on confocal imaging, *Journal of Modern Optics*, **43**, 469-486.

[10] **Schatzberg, A., Devaney, A.J.,** 1993. Rough surface inverse scattering within the Rytov approximation, *Journal of the Optical Society of America*. **A 10,** 942–950.

[11] **Spivack, M.,** 1992. Direct solution of the inverse problem for rough surface scattering at grazing incidence, *Journal of Physics. A: Mathematical and General*, **25,** 3295-3302.

[12] **Wombell, R.J., DeSanto, J.A.,** 1991. The reconstruction of shallow rough-surface profiles from scattered field data, *Inverse Problems,* **7**, L7–L12**.**

[13] **El-Shenawee, M., Miller, E.L.,** 2004. Multiple-incidence and multifrequency for profile reconstruction of random rough surfaces using the 3D electromagnetic fast multipole model, *IEEE Transactions on Geoscience and Remote Sensing,* **42**, 2499–2510.

[14] **Galdi, V., Pavlovich, J., Karl, W.C., Castanon, D.A., Felsen, L.E.,** 2003. Moderately rough dielectric interface profile reconstruction via short-pulse quasi-ray Gaussian beams, *IEEE Transactions on Antennas and Propagation,* **51,** 672-677.

[15] **Stankova, M., Burov, J., Burova, M.,** 2001. Computer reconstruction of a periodic surface by means of the scattered and transmitted acoustic fields, *Measurement Science and Technology*, **12**, 1330-1335.

[16] **Akduman, I., Kress, R., Yapar, A.,** 2006. Iterative Reconstruction of Dielectric Rough Surface Profiles at Fixed Frequency, *Inverse Problems*, **22**, 939-954.

CURRICULUM VITAE

Çağla Taşdemir was born in Zonguldak, Turkey, in 1984. She received her B.Sc. degree in Telecommunication engineering from Istanbul Technical University in 2006. Currently, she is a member of Elecromagnetic Research Group in ITU and working toward her M.Sc. degree.